

Columnar liquid crystals formed by bowl-shaped mesogens. A Monte Carlo study

Matteo Ricci, Roberto Berardi, and Claudio Zannoni[°]

Dipartimento di Chimica Fisica e Inorganica, and INSTM-CRIMSON,

Università di Bologna,

Viale Risorgimento 4, 40136 Bologna, Italy

[°] email: Claudio Zannoni <claudio.zannoni@unibo.it>

[version Sunday, June 1, 2008]

Received XXXXth March, 2008

Accepted XXXXth Month, 2008

DOI: 10.1039/

We have investigated the stacking of model bowl-shaped mesogens, and the nematic and columnar liquid crystal phases they form upon cooling-down from an isotropic liquid. Starting from an attractive-repulsive interaction obtained generalising the Gay-Berne pair potential to bowl-shaped mesogens, we have performed extensive off-lattice Monte Carlo NPT computer simulations of samples of various sizes: $N = 1024, 8192, \text{ and } 32000$ particles. We have examined in particular the length of the polar domains formed and their polydispersity, and characterised in detail the structure of the packing defects terminating the columns.

1 Introduction

The self assembly of suitable molecules in ordered structures is a powerful approach toward building components and devices for organic electronics [1]. In particular flat shape (“discotic”) mesogens have been employed to build columnar stacks for applications in organic transistors and photovoltaics [2] exploiting their strongly anisotropic transport properties. Since the discovery of the first discotics, some thirty years ago [3], a variety of flat mesogens have been prepared [4, 2], particularly in the effort of improving their electronic properties, e.g. to-

wards optimal conductivity.

Very interesting features of these systems are that molecular columns are formed spontaneously, just by changing temperature or by solvent evaporation, like in spin coating procedures, and that these structures can self anneal. Indeed, being to some extent fluids, columnar phases should avoid, e.g., the problem of grain boundaries which vexes the use of crystalline organic materials. Unfortunately, the discotic columns also present irregularities, in particular the molecular stacking in columns is interrupted by defects, e.g. discs slipping from the columns, or swallow tail doubling of the columns. When choosing mesogens that can stack an important problem is thus that of controlling the size of these columns. Using concave, bowl-shaped rather than flat shaped mesogens should intuitively be expected to improve stacking. Indeed, the idea of using bowl-shaped molecules has been around for quite some time, particularly to try and build achiral ferroelectric liquid crystal materials [5, 6, 7, 8, 9]. In that case, the expectation is that if each bowl-shaped molecule has an axial dipole, they should pile up head to tail yielding a macroscopic column dipole. The formation of an hexagonal columnar phase, as often found in columnar discotics would ensure an overall ferroelectric order [9, 10]. A variety

of bowl-like mesogens have been put forward, e.g. based on tribenzocyclononenes [11], metallorganic compounds [5, 7], cyclotryveratrilene [12], calix[4]arenes [13, 14], and C₆₀ fullerene derived molecules [15]. In the latter case the shape is somewhat different but the C₆₀ apex of each of these molecules fits perfectly into the cavity of a neighbouring one.

Despite the flourishing of synthetic work and of the attendant characterisation activity, modelling and simulation studies have been very limited. A detailed atomistic simulation of the type that has recently been successfully applied to describing low molar mass nematics [16, 17, 18] is clearly currently unfeasible for molecules as complicated as the bowl-like mesogens mentioned above. At the other extreme, lattice models with a combination of polar and quadrupolar symmetry have been simulated [19] and polar regions of the phase diagram have been described. Essentially the same potential has also been studied with Mean Field Theory [20]. However, a strong limitation of these treatments is the absence of anisotropic repulsive shape effects, that are key to the piling of bowls. Very recently a coarse-grained soft-core model based on approximating complex conical fullerene mesogens with a set of cubic building blocks with rotations and translations restricted to a lattice has been successfully put forward [21]. The more realistic and very effective off-lattice molecular resolution type approach, where a complex molecule is replaced by a simple object like an ellipsoid or a spherocylinders [22, 23, 17], interacting via attractive-repulsive pair potentials, has extensively been employed for discotics, but cannot be applied, as such, to bowl-like particles. On the other hand we have shown that particles of other shapes, e.g. tapered ones [24, 25], can be effectively studied by suitably approximating their contact distance [26] as a function of the relative position and of the orientation of the interacting particles.

Here we plan to develop a simple molecular model for bowl-shaped molecules and to perform a series of MC simulations of their phase behaviour. Since there is very little theoretical modelling for these type of systems we believe

that such a study is essential in establishing a relation between molecular features and columnar organisation, clarifying the role of shape and attraction in bowl-like systems. As a first objective we plan to examine the possibility of getting long columnar stacks as opposed to just short domains without long range correlation. We also wish to see how the columns are terminated, and the nature of the resulting structural defects.

2 Modelling

We represent uniaxial bowl-shaped molecules using a combination of attractive and repulsive pair interactions with the help of a methodology we have already employed in Ref. [24], based on a generalisation of the Gay-Berne (GB) potential [27, 28]. This off-lattice potential is the *de-facto* standard model for the simulation at molecular resolution of a variety of liquid crystals [22, 23, 17], and has the advantage of simplicity since it consists of only one site per molecule. Here we are particularly interested in the effect of the particle shape on the macroscopic properties, and we shall model the repulsive part of the potential in terms of the anisotropic contact distance. To this effect we represent the bowl conical particles shape as the solid of rotation from the 2 π revolution of a two-dimensional cross-section (see Fig. A-1). This profile has in turn been obtained by joining four parametric Bezier curves [29] defined in terms of the control points listed in Table A-1. As in Ref. [26, 24], we expand the pair contact distance computed numerically (see Fig. 1 for a schematic description of our methodology) as

$$\sigma(\mathbf{u}_1, \mathbf{u}_2, \mathbf{u}_r) = \sum_{L_1 L_2 L_3} \sigma_{L_1 L_2 L_3} S^{L_1 L_2 L_3 *}(\mathbf{u}_1, \mathbf{u}_2, \mathbf{u}_r) \quad (1)$$

where σ_{L_1, L_2, L_3} are the expansion coefficients, and the S^{L_1, L_2, L_3} are a suitable set of rotational invariant orthogonal functions [30, 31, 32] for the orientations $\mathbf{u}_1, \mathbf{u}_2$ of the two molecules (given as unit vectors), and that \mathbf{u}_r of the intermolecular vector $\mathbf{r}_{12} = r_{12}\mathbf{u}_r$.

Here we consider bowl-shaped particles (see Fig. A–1) of width $w = 0.75 \sigma_0$, and length $l = 0.675 \sigma_0$, with σ_0 the unit of distance. Using these dimensions the vertical distance h between base and molecular frame (see Fig. A–1) is $h = 0.3 \sigma_0$. In Table A–2 we list the 49 expansion coefficients σ_{L_1, L_2, L_3} used to approximate the pair contact distance for a pair of bowl-shaped particles. The sections of the contact distance are well reproduced by the approximating expansion with an overall relative error of a few percent units (see Fig. 2). The contact distance expansion $\sigma(\mathbf{u}_1, \mathbf{u}_2, \mathbf{u}_r)$ accounts for shape anisotropy in the generalised Gay–Berne potential

$$U(\mathbf{u}_1, \mathbf{u}_2, \mathbf{r}_{12}) = 4\epsilon_0 \epsilon(\mathbf{u}_1, \mathbf{u}_2, \mathbf{u}_r) \times \left[\left(\frac{\sigma_c}{r_{12} - \sigma(\mathbf{u}_1, \mathbf{u}_2, \mathbf{u}_r) + \sigma_c} \right)^{12} - \left(\frac{\sigma_c}{r_{12} - \sigma(\mathbf{u}_1, \mathbf{u}_2, \mathbf{u}_r) + \sigma_c} \right)^6 \right] \quad (2)$$

where we take the interaction range parameter as $\sigma_c = 0.158 \sigma_0$, and ϵ_0 is the unit of energy. Since in this study we are mainly interested in assessing the effects due to shape anisotropy alone, we have chosen a centrosymmetric attraction term $\epsilon(\mathbf{u}_1, \mathbf{u}_2, \mathbf{u}_r)$ that brings the molecules closer without any energetic preference for *top-to-top*, *top-to-base*, or *base-to-base* interactions (see Fig. 3). In practice, the interaction term $\epsilon(\mathbf{u}_1, \mathbf{u}_2, \mathbf{u}_r)$ in equation 2, is modelled by using the centrosymmetric expression reported in Ref. [24], with coefficients $\epsilon_{000} = 81.25$, $\epsilon_{101} = 0$, $\epsilon_{011} = 0$, $\epsilon_{220} = -1.25$, $\epsilon_{202} = 3.75$, $\epsilon_{022} = 3.75$, $\lambda_{110} = 0$, $\lambda_{220} = 1.5$, and $\lambda'_{220} = 0$.

3 Monte Carlo simulations

We have performed off-lattice Monte Carlo (MC) simulations of a system of bowl-shaped mesogens described above in the isobaric-isothermal (MC–NPT) ensemble at dimensionless pressure $P^* = \sigma_0^3 P / \epsilon_0 = 8$, simulating bulk samples of $N = 1024$, and 8192 particles modelled with the coarse-grained pair potential described before, and considering a wide range of dimensionless temperature $T^* = k_B T / \epsilon_0$.

Some runs have also been performed on larger samples of $N = 32000$ particles. The sampling ranges for the standard MC moves were adjusted run-time to give an average acceptance ratio of 40% at all temperatures, ranging between $0.01 \sigma_0$ and $0.05 \sigma_0$ for translations, and 2° and 10° for rotations. The phase diagram has been explored performing sequences of both cooling-down and heating-up MC runs, starting each simulation from a configuration well equilibrated at the previous temperature. We have found isotropic (*I*), nematic (*N*), and columnar (*C*) phases. We should remark that systems formed by bowl-shaped molecules are experimentally known to give rise to glassy-like materials [7], and this behaviour does make the computation of statistically reliable thermodynamic properties very demanding because the equilibration stage of the simulation is slowed down by the many local free energy minima typical of the highly structured columnar organisations which are visited during the MC evolution, and that are difficult to unlock. To enhance the MC sampling efficiency and to avoid the formation of artifacts (e.g. cavities) in the lower temperature samples we have used a triclinic simulation box [33] with three-dimensional periodic boundary conditions, allowing box sides and shape to evolve independently during both MC equilibration and production runs. To reduce the chance of being trapped in metastable glassy phases, we have augmented the standard set of randomly attempted translational and orientational MC moves with both *top-base* flips of particles, and whole column cluster moves. The first kind of extended MC moves [34] attempts to exchange particle top with base by performing a 180° rotation around the molecular *y* axis. Such flip moves have been randomly attempted with an average 0.2 probability compared to the standard rotational-translational MC moves, and with average acceptance ratios ranging from 1% for the lowest T^* up to 12% for the highest temperatures. The second kind of extended MC moves randomly attempts collective roto-translations and *top-base* flip of clusters [34, 35] of particles (i.e. entire columns or stacks), with average acceptance ratio 1%, and sampling ranges $0.003 \sigma_0$ to $0.004 \sigma_0$ for trans-

lations, and 0.7° to 1° for rotations.

After equilibration the average thermodynamic observables have been computed sampling a configuration every 20 MC cycles, with one cycle being a random sequence of N attempted MC moves. Very long simulation runs, compared to the standard employed for molecular resolution models [22] have been employed: the equilibration runs were at least 400 kcycles, while typical production runs were considerably longer (up to 1000 kcycles). Using the results of a preliminary set of exploratory MC simulations on the smallest ($N = 1024$ particles) system, we have sampled the temperature points of the $N = 8192$ sample over a non uniform grid, using a slightly finer mesh in the proximity of phase transitions. Only selected temperatures have been studied for the largest $N = 32000$ sample size. In the following section we report results from MC-NPT simulations following a cooling-down sequence, starting from a well equilibrated isotropic sample at $T^* = 1.6$.

4 Results and discussion

We start from the principal features of the phase diagram for the system. Considering the average adimensional enthalpy $\langle H^* \rangle = \langle H \rangle / \epsilon_0$ measured in a cooling-down temperature scan (see Figs. 4–A, and Table 1) we observe that the system first undergoes at $T^* = 1.45$ a weak transition to nematic, shortly followed at $T^* = 1.38$ by a second one to a columnar structure. The transition temperatures have been estimated as the midpoint between the last temperature of a previous phase and the first of a following one. We have based our discussion on a cooling-down sequence from isotropic because this protocol usually gives more reliable results for the ordering in self-assembling processes. We note that the range of stability for the nematic phase is rather narrow, possibly because the shape anisotropy strongly favours molecules packing into densely stacked clusters.

The spontaneous onset of orientational and positional ordering appearing from the MC cooling runs is associated with a large increase in density due to the stacking-up of particles. The

average number density $\langle \rho^* \rangle = \sigma_0^3 N \langle 1/V \rangle$ of Fig. 4–B and Table 1 shows first a substantial increment at the nematic transition and then an even larger increase (from $\langle \rho^* \rangle = 3.4$ to 4.5) when the columnar transition temperature is reached. The density shows instead a decrease at even lower temperatures, highlighting the difficulty of fully packing the sample, at least in a cooling run and in the absence of an external orienting field. This can be interpreted as due to the formation of a multi-domain structure of densely packed columns oriented in different directions. The typical features of the low temperature organisations are apparent from the snapshot of Fig. 6–A which clearly shows a liquid crystalline structure formed by small domains of polar columns.

The onset of orientational ordering in liquid crystalline phases is determined with the second rank order parameter $\langle P_2 \rangle = \langle (3(\mathbf{u}_i \cdot \mathbf{n})^2 - 1)/2 \rangle$, expressing the average orientation of the molecular axis \mathbf{u}_i with respect to the mesophase director \mathbf{n} . The order parameter is computed with the standard algorithm [36, 37] employed in liquid crystals computer simulations from the largest eigenvalue of a sample averaged ordering matrix $\mathbf{Q} = \langle 3\mathbf{u}_i \otimes \mathbf{u}_i - \mathbf{I} \rangle / 2$ [36]. The diagonalisation of \mathbf{Q} provides also the direction of \mathbf{n} from the corresponding eigenvector.

As we lower the temperature, the average order parameter $\langle P_2 \rangle$ (plotted in Fig. 5–A, and reported in Table 1) shows a discontinuity when the nematic ordering transition takes place. For the smaller $N = 1024$ sample the order increases upon reducing T^* . Surprisingly, for a further reduction of temperature the overall order parameter in the larger $N = 8192$, and 32000 samples does not increase as it is expected in thermotropic LC, but rather it even decreases or levels to a plateau value. This unusual behaviour, connected to that already seen in the density, corresponds to the columns not being globally oriented in space. We point out that in a multidomain system the overall average $\langle P_2 \rangle$ can be written as a product of the order parameters for the molecules inside the columns (measured with respect to each column principal axis), and an order parameter giving the average alignment of the column axes with respect

to the overall director $\langle P_2 \rangle = \langle P_2 \rangle_{\text{axes}} \langle P_2 \rangle_{\text{intra}}$. In Fig. 5–B we show the order of the molecules with respect to their column axis. We see that the order parameter inside the columns $\langle P_2 \rangle_{\text{intra}}$ increases regularly decreasing the temperature, as expected. We also see that increasing system size the isotropic–nematic transition is slightly shifted to lower temperatures.

The knowledge of the director \mathbf{n} allows the direct computation of other order parameters. For instance, to assess if the samples spontaneously gained an overall net polarisation we have also computed the average first rank Legendre polynomial $\langle P_1 \rangle = \langle \mathbf{u}_i \cdot \mathbf{n} \rangle$, also shown in Table 1. For all temperatures explored by the MC–NPT simulations the $\langle P_1 \rangle$ order parameter was always zero, so we conclude that at the microscopic scale explored by the MC simulations our system of bowlic particles does not spontaneously polarise. This is similar to what has been found by Photinos and coworkers with a soft–core lattice model of conical mesogens [21]. We can immediately see (with the help of a colour coding of the particles orientation, see Fig. 6–C), that the number of upward and downward oriented polar columns is balanced. The piling up of *top–to–base* pairs leads to build–up of polar order inside a column, until this stacking terminates with a *top–to–top* or *base–to–base* pair (i.e. a defect), or a boundary surface separating neighbouring domains. This kind of positional structuring is essentially absent in the nematic phase (see Fig. 6–B) where the large majority of particle stacks is not longer than three units.

We notice that the columnar aggregates are not permanent. We have checked the reversibility of the spontaneous self assembling process by heating the lowest temperature sample directly above the nematic–isotropic transition, and we have observed a large volume increase associated to column disassembling. By conducting instead gradual heating runs from an intermediate temperature columnar system, we have found considerable hysteresis effects in the phase diagram, before the isotropic eventually appears, related to the different multi–domain structure of the samples which can not be controlled. Nonetheless we note that the intra–

columnar order is comparable in both cases (see Fig. 5–B).

In view of the large temperature dependence of the number density, and to assess whether our simulations produced fluid ordered phases and not solid structures, we have calculated the root mean square translational displacements $\langle \Delta r^2 \rangle_a^{1/2}$ along directions parallel and perpendicular to the mesophase director \mathbf{n} (see Fig. 7)

$$\ell \equiv \langle \Delta r^2 \rangle_a^{1/2} = \left\{ \sum_i^N \sum_n^M \frac{[r_{i,a}^{(n)} - r_{i,a}^{(0)}]^2}{NM} \right\}^{1/2} \quad (3)$$

where $a = \parallel$, or \perp refers to the particles position with respect to the director frame after n of M MC cycles starting from an arbitrary initial point. We have found small mobilities with values comparable with those of other columnar model systems (e.g. discotic Gay–Berne samples [38]) and down to $\ell \simeq 0.15$ [39], solid–like according to the standard Lindemann type criterion [39]. These root mean square displacements increase steadily with temperature, with nematic being fluid. The most unexpected result was that in both nematic and columnar phases we did not observe a net anisotropy between the parallel and perpendicular components. This can be interpreted once more as associated with the formation of a uniform distribution of multi–domain columnar structures (see Fig. 6–A).

The essential features of short–range positional correlations typical of specific anisotropic ordered structures can be assessed analysing the radial correlation function

$$g_0(r) = \langle \delta(r - r_{12}) \rangle_{12} / (4\pi^2 \rho) \quad (4)$$

where the angular brackets $\langle \dots \rangle_{12}$ notation stands for an ensemble average over all particle pairs. Thus, $g_0(r)$ allows to discriminate between the typical short–range positional order in the nematic and columnar phases. The radial correlation function for the nematic phase (shown in Fig. 8–B) is characterised by a very limited short–range structuring. At these temperatures $g_0(r)$ is very similar to those of discotics systems [38], with the concave shape of

the particles only determining a small peak at $r^* = 0.25$. The probability of observing a pair of molecules at distances corresponding to stacked structures comprising more than three units is fairly small, in agreement with the qualitative conclusions drawn inspecting Fig. 6–B. The only signature for local positional ordering has been measured for distances typical of *side-by-side* configurations (with $r^* \approx 0.8$). The $g_0(r)$ for the isotropic phase (not shown here) is qualitatively similar to that for the nematic phase but with even smaller short-range density probability of pairs.

In the columnar phase the molecular organisation is strongly affected by the bowlic shape of the particles and we see from Fig. 8–A that at distances $r^* \approx 0.2$ corresponding to a *top-to-base* sequence of stacked molecules with parallel orientation (see Fig. 2–A, with θ_r either 90° , or 270°) the $g_0(r)$ histogram has a sharp peak. The second peak is for $r^* \approx 0.8$ which corresponds to parallel and anti-parallel molecules *side-by-side* (see Figs. 2–A and 2–D, with θ_r either 0° , or 180°) belonging to neighbouring columns.

Some further insights on the short-range polar arrangements can be derived by the first rank orientational correlation $S^{110}(r) = -\langle \delta(r - r_{12}) \mathbf{u}_1 \cdot \mathbf{u}_2 \rangle_{12} / \sqrt{3}$ (see Figs. 8–A and 8–B) which for distances corresponding to highly aligned parallel molecules in a *top-to-base* configuration and, apparent for all temperatures, has a sharp drop from zero towards the boundary -0.57 value. The distance range spanning this negative portion of the correlation function is smallest in the isotropic phase (not shown here), and increases regularly when reducing the temperature and after an ordering phase transition. The short-range polar correlations are meaningful (in the sense of being associated with a relevant population of pairs) only for the columnar phase, because in the isotropic and nematic phases the $g_0(r)$ values for these separations are fairly small. For larger distances involving sampling regions which extend even over antiparallel pairs belonging to neighbouring columns, the average correlation becomes first weakly positive, and then for all temperatures averages to zero. This is especially the case for distances where the nematic and isotropic radial correla-

tions have the absolute maximum. Even these correlations support (in agreement with the $\langle P_1 \rangle$ values of Table 1) the picture that this system does form polar columnar assemblies, but is devoid of an overall net polarisation.

An essential part of the present work is to investigate the molecular organisation in columns and the first step is to decide if a molecule belongs to a column or not. To this purpose we have contrived a simple algorithm to map stacked pairs and identify one-dimensional columnar structures. Two particles are defined as jointly stacked if all these conditions are simultaneously met: (a) the pair distance r_{12} is smaller than $0.5 \sigma_0$; (b) the angle between particle orientations $\mathbf{u}_1, \mathbf{u}_2$ is smaller than 30° ; and (c) both angles between the intermolecular vector \mathbf{r}_{12} and the particles orientations $\mathbf{u}_1, \mathbf{u}_2$ are smaller than 35° . By using these heuristic parameters, a particle can at most be labelled as linearly stacked with two other molecules (one “above”, and one “below”). A column of length n_p particles can then be defined as a collection of $n_p - 1$ chained pairs with repeated labels. When analysing the MC configurations, to avoid averaging properties originating from unstable structures, we define a column as a stack containing not less than 4 particles. Using these empirical parameters we never observe occurrences of columnar aggregates in the isotropic phase.

The previous algorithm, specific for linearly stacked aggregates, provided a list of columns which has been used to compute ensemble averages and histograms on every MC configuration produced by the MC simulations. We report in Fig. 9 the number n_c of columns formed by n_p particles for some selected temperatures of the nematic and columnar phases. The distribution for the nematic phase at $T^* = 1.4$ shows the presence of a limited average number of fairly short stacks. On the other hand, the histograms at $T^* = 1.37$, and $T^* = 1.25$ tell us that in the columnar phase a rich population of one-dimensional structures appears. In both cases the shape of the distributions is similar, with a maximum corresponding to very short columns. This portion of the histogram has the larger temperature dependence, while

the tails of the distributions do not substantially differ between the samples at $T^* = 1.37$, and $T^* = 1.25$. This is consistent with a picture of a thermotropic columnar transition where the principal structuring in ordered domains, with tens of stacked molecules for every column, immediately takes place when the nematic phase becomes relatively unstable. The subsequent lowering of temperature mostly affects the fraction of isolated molecules which pair to form short supramolecular structures or possibly enlarge existing ones. To further clarify this anisotropic structuring we report in Table 2 the temperature dependence of the average fraction of particles belonging to columns $\langle x_c \rangle$, as well as the average number of particles per column $\langle n_p \rangle$ (in terms of number of units forming an ordered stack), and the average number of columns $\langle n_c \rangle$. The average $\langle n_p \rangle$, and $\langle n_c \rangle$ values are fairly small in the isotropic and nematic phases, even though the fraction $\langle x_c \rangle$ roughly doubles when the liquid crystalline phase transition takes place. A further reduction of temperature induces a dramatic increase in the average number $\langle n_c \rangle$ and length $\langle n_p \rangle$ of columnar structures, which remain afterwards constant with respect to T , as also does the fraction $\langle x_c \rangle$.

Having mapped all ordered aggregates it is possible to compute the radial correlation function using a column-wise sampling of $g_0(r)$ where molecular pairs at a given distance are included only when they belong to the same stacked structure. This overcomes the problems arising with the standard sampling over spherical shells, which smooths out many details of the complex highly anisotropic structures of our type of systems. In Fig. 10–A we observe quite a different shape in the pair correlation histograms when using this column-wise sampling scheme. The structuring is negligible in the isotropic and nematic systems (see inset of Fig. 10–A), while in the columnar phase the first- and second-neighbour maxima are fairly well defined. For longer distances, the $g_0(r)$ decreases without further evidences of regular structuring. This can be interpreted in view of the smaller population of longer stacks (see Fig. 9), but also from the presence of many not linear stacks, like the one shown in Fig. 10–B,

where the winding sections have different spacing between stacked particles which smooths out the regular sequence of maxima and minima in the density distribution.

The second level of supramolecular organisation, i.e. the assembling of columns into polar domains, see e.g. Fig. 11, was quite surprising. In fact, while the one-dimensional stacking effect was expected from simple considerations about the bowl shape of the steric dipoles, the structuring of columns into polar domains was not immediately recognised as related to this feature. This property is not originated from the specific anisotropy of the attractive part of the pair potential (see Fig. 3), because the energy surface is centro-symmetrical and neighbouring parallel or antiparallel columns would have the same interaction. An additional step necessary for the characterisation of these structures was the setting up of a specific procedure aimed at mapping polar columnar domains. Two stacks are mapped as forming an inter-columnar assembly if these two conditions are simultaneously met: (a) the distance between the columns centres of mass is smaller than $1.5 \sigma_0$; and (b) the angle between column orientations, which has been defined as the normalised average of its particle orientations, is smaller than 15° . Using this procedure all structures without a globular shape (e.g. single threads) were not taken into account. Again, to refrain from averaging contributions stemming from strongly fluctuating structures, the minimum number of neighbouring columns to be accounted as forming a domain has been set to 3. The distributions of the number n_d of domains formed by the grouping of n_c columns are shown in Fig. 12. We observe for the lowest temperatures a scattered population, where more than 98% of the total number of particles organised in columnar structures are formed by up to 20 stacks. A lowering of temperature from $T^* = 1.37$ to $T^* = 1.25$ introduces a significant population increase also in the low n_c histogram bins corresponding to domains formed by tens of stacks. We conclude that the major effect of temperature on the columnar phase is that of strongly increasing the inter-column correlations, while the intra-column structure is

less influenced. The histogram for $T^* = 1.4$ in Fig. 12 shows that the nematic phase is practically devoid of columnar clusters larger than 3 stacks. The outcome from the structural analysis of columnar domains for the various temperatures is summarised in Table 3 where we report the average fraction of columns organised in domains $\langle x_d \rangle$, the number of domains $\langle n_d \rangle$, and the number of columnar stacks per domain $\langle n_s \rangle$. The average fraction $\langle x_d \rangle$ is practically zero in the isotropic and nematic phases, and becomes larger than 80% after the columnar phase transition. This is consistent with the discussion of the distributions of Fig. 12. Once the stacks assemble and form domains, the average fraction $\langle x_d \rangle$ does not change much with temperature. This constant behaviour arises from two ordering processes with opposite trends. The average number of domains $\langle n_d \rangle$ of Table 3 steadily increases when lowering the temperature, while the number of columns within each domain decreases on average. This can be interpreted with an increase in internal ordering within each domain accompanied by the coalescing of smaller stacks to form longer ones (see also Fig. 12).

In order to understand the molecular origin of the polar domains, we have studied the typical structure of the boundary between regions with opposite polarities (see Fig. 11). We have found a systematic interleaving spacing between column ends of neighbouring clusters with *top-to-top* boundary structure (see the geometrical sketches in Figs. 13–A and 13–B). The columns of both confining regions match their orientations by displacing laterally with respect to the common direction of polar alignment. This top–column particle coordination of neighbours favours the formation of stacks with opposite polarity in the adjacent domain. To verify more quantitatively this observation we have computed correlation functions specifically considering only pairs of particles at the end of different stacks (those ending their column with a cusp). In Fig. 14–A we report the radial $g_0(r_{end})$, and the orientational particle–particle $S^{110}(r_{end})$ and particle–intermolecular vector $S^{101}(r_{end}) = -\langle \delta(r_{end} - r_{12}) (\mathbf{u}_1 \cdot \mathbf{u}_r) \rangle_{end-12} / \sqrt{3}$ correlation functions. The symbol r_{end} represents the distance between end–particles of dis-

tinct stacks. The pictorial scheme of Fig. 14–B helps in assigning the various local maxima of the correlation functions to specific configurations of end–particles belonging to different columns at various distances. The spacing of the alternated sequence of maxima and minima for the $S^{110}(r_{end})$ correlation (see red dashed curve in the inset of Fig. 14–A) is consistent with the proposed boundary structure of intercalated end–particles with opposite orientation (see also Figs. 2–A, and 2–D).

4.1 Conclusions

We have studied the formation of columnar structures in a system of bowl–shaped molecules using off–lattice computer simulations. To model concave particles we have generalised the molecular resolution Gay–Berne potential via a suitable series expansion for two bowl–shaped molecules. The MC–NPT simulations we have run with this model showed that its particular shape induces two types of polar ordering: one dimensional order along columns of stacked particles, and organisation in three-dimensional polar clusters of parallel columns. In our case attraction anisotropy can hardly play any role in polar ordering, because we have chosen a centro–symmetrical attractive part of the GB potential. However, the polar stacks do not extend across the whole sample, and we do not observe a net overall polarisation. We have characterised these two levels of supramolecular ordering by defining heuristic procedures to identify and map columns and coherent domains of stacks. The first ordering effect was easily predictable from geometrical considerations about the bowl shape giving rise to piling up in stacks, but the second was quite unexpected. We have proposed a mechanism for the formation of polar domains which again relies on the shape anisotropy of our model particles. The defects terminating the columns can be explained by the coordination effect of the columns tips on antiparallel particles in contact with them. This effect arises from the packing of column ends at the boundary between domains assembling with opposite polarity, and provides an effective way of terminating columns. This

defect stabilisation in turn indicates that changing from discotic to bowlic shape may be insufficient to ensure very long coherent molecular stacks as needed to optimise transport in organic electronic devices, supporting the need for more specific attractive interactions to stabilise polar domains.

Acknowledgements

We thank MUR, INSTM, and EU-STREP “Modelling electro-active conjugated materials at the multiscale” (MODECOM #NMP3-CT-2006-016434) for financial support.

Reference

References

- [1] I. W. Hamley. Nanotechnology with soft materials. *Angew. Chem. Int. Ed.*, 42:1692, 2003.
- [2] S. Sergeev, W. Pisula, and Y. H. Geerts. Discotic liquid crystals: A new generation of organic semiconductors. *Chem. Soc. Rev.*, 36:1902, 2007.
- [3] S. Chandrasekhar. *Advances in Liquid Crystals*, volume 5. Academic Press, NY, 1982.
- [4] R. J. Bushby N. Boden and O. R. Lozman. Designing better columnar mesophases. *Molec. Cryst. Liq. Cryst.*, 400:105, 2003.
- [5] J.L. Atwood, L.J. Barbour, M.J. Hardie, and C. Raston. Metal sulfonato-calix[4,5]arene complexes: bi-layers, capsules, spheres, tubular arrays and beyond. *Coordination Chemistry Review*, 222:3–32, 2001.
- [6] J. Malthête and A. Collet. *J. Am. Chem. Soc.*, 109:7544, 1987.
- [7] B. Xu and T. M. Swager. *J. Am. Chem. Soc.*, 115:1159, 1993.
- [8] L. M. Blinov. On the way to polar achiral liquid crystals. *Liq. Cryst.*, 24:143, 1998.
- [9] D. Guillon. Molecular engineering for ferroelectricity in liquid crystals. *Adv. in Chemical Physics*, 113:1, 2000.
- [10] C. Tschierske. Liquid crystals stack up. *Nature*, 419:681–683, 2002.
- [11] H. Zimmermann, R. Poupko, Z. Luz, and J. Billard. Pyramidic mesophases. *Z. Naturforsch. A.*, 40:149, 1985.
- [12] G. Cometti, E. Dalcanale, A. Duvosel, and A. M. Levelut. A new, conformationally mobile macrocyclic core for bowl-shaped columnar liquid-crystals. *Liq. Cryst.*, 11:93, 1992.
- [13] I. D. Demus. *Liq. Cryst.*, 5:75, 1989.
- [14] T. M. Swager and B. Xu. Liquid-crystalline calixarenes. *J. Incl. Phenom. Mol. Recogn. Chem.*, 19:389, 1994.
- [15] M. Sawamura, K. Kawai, Y. Matsuo, K. Kanie, T. Kato, and E. Nakamura. Stacking of conical molecules with a fullerene apex into polar columns in crystals and liquid crystals. *Nature*, 419:702–705, 2002.
- [16] R. Berardi, L. Muccioli, and C. Zannoni. Can nematic transitions be predicted by atomistic simulations? a computational study of the odd-even effect. *ChemPhysChem*, 5:104, 2004.
- [17] M. R. Wilson. Progress in computer simulations of liquid crystals. *Int. Rev. Phys. Chem.*, 24(3 & 4):421–455, 2005.
- [18] Jorge Peláez and Mark R. Wilson. Atomistic simulations of a thermotropic biaxial liquid crystal. *Phys. Rev. Lett.*, 97(26):267801, 2006.
- [19] F. Biscarini, C. Zannoni, C. Chiccoli, and P. Pasini. Head tail asymmetry and ferroelectricity in uniaxial liquid-crystals. model-calculations. *Molec. Phys.*, 73:439, 1991.
- [20] L. Lei. Bowlic liquid crystals. *Molec. Cryst. Liq. Cryst.*, 146:41, 1987.

- [21] S.D. Peroukidis, A.G. Vanakaras, and D.J. Photinos. Self-organisation of fullerene-containing conical supermesogens. *Soft Matter*, 4:493–499, 2008.
- [22] C. Zannoni. Molecular design and computer simulations of novel mesophases. *J. Mater. Chem.*, 11(11):2637–2646, 2001.
- [23] C. M. Care and D. J. Cleaver. Computer simulation of liquid crystals. *Reports on Progress in Physics*, 68(11):2665–2700, 2005.
- [24] R. Berardi, M. Ricci, and C. Zannoni. *ChemPhysChem*, 2:443, 2001.
- [25] F. Barmes, M. Ricci, C. Zannoni, and D.J. Cleaver. Computer simulations of hard pear-shaped particles. *Phys. Rev. E*, 68(2):021708, 2003.
- [26] H. Zewdie. Computer simulation studies of liquid crystals: A new corner potential for cylindrically symmetric particles. *J. Chem. Phys.*, 108:2117, 1998.
- [27] J. G. Gay and B. Berne. A monte carlo simulation study of associated liquid crystals. *J. Chem. Phys.*, 74:3316, 1981.
- [28] R. Berardi, A. P. J. Emerson, and C. Zannoni. Monte carlo investigations of a gay-berne liquid crystal. *J. Chem. Soc. Faraday Trans.*, 89:4069–4078, 1993.
- [29] J. D. Foley and A. Van Dam. *Fundamentals of Interactive Computer Graphics*. Addison-Wesley, Reading, Massachusetts, 1982.
- [30] L. Blum and A. J. Torruella. *J. Chem. Phys.*, 56:303, 1972.
- [31] A. J. Stone. *Molec. Phys.*, 36:241, 1978.
- [32] S. L. Price, A. J. Stone, and M. Alderton. *Molec. Phys.*, 52:987, 1984.
- [33] S. Yashonath and C. N. R. Rao. Molecular design and computer simulations of novel mesophases. *Molec. Phys.*, 54:245, 1985.
- [34] D. Frenkel and B. Smit. *Understanding Molecular Simulations, 2nd edition*. Academic Press, San Diego, 2001.
- [35] R. Berardi, M. Fehervari, and C. Zannoni. A monte carlo simulation study of associated liquid crystals. *Molec. Phys.*, 97:1173–1184, 1999.
- [36] C. Zannoni. Distribution function and order parameters. In G. R. Luckhurst and G. W. Gray, editors, *The Molecular Physics of Liquid Crystals*, chapter 3, pages 51–83. Academic Press, London, 1979.
- [37] C. Zannoni. Quantitative description of orientational order: rigid molecules. In J.W. Emsley, editor, *Nuclear Magnetic Resonance of Liquid Crystals*, pages 1–34. Reidel, Dordrecht, 1985.
- [38] R. Berardi, S. Orlandi, and C. Zannoni. Monte carlo simulations of discotic gay-berne mesogens with axial dipole. *J. Chem. Soc. Faraday Trans.*, 93:1493–1496, 1997.
- [39] Frank H. Stillinger. A Topographic View of Supercooled Liquids and Glass Formation. *Science*, 267(5206):1935–1939, 1995.

Table 1: Average orientational order parameter $\langle P_2 \rangle$, dimensionless enthalpy $\langle H^* \rangle$, and number density $\langle \rho^* \rangle$ for the MC–NPT simulations of the $N = 8192$ system giving isotropic (I), nematic (N), and columnar (C) phases as indicated. Estimated rms errors on the averages (sampling a configuration every 20 MC cycles) are also given.

T^*	$\langle P_2 \rangle$	$\langle P_1 \rangle$	$\langle H^* \rangle$	$\langle \rho^* \rangle$	phase
1.25	0.52 ± 0.05	0.004 ± 0.013	-9.89 ± 0.20	4.33 ± 0.18	C
1.30	0.57 ± 0.04	0.023 ± 0.012	-9.66 ± 0.31	4.53 ± 0.19	C
1.35	0.55 ± 0.19	0.003 ± 0.013	-9.20 ± 0.71	4.30 ± 0.31	C
1.37	0.62 ± 0.06	0.035 ± 0.016	-8.46 ± 0.54	3.95 ± 0.21	C
1.40	0.65 ± 0.01	0.001 ± 0.008	-4.28 ± 0.09	3.39 ± 0.02	N
1.42	0.59 ± 0.01	0.000 ± 0.009	-3.60 ± 0.09	3.24 ± 0.02	N
1.44	0.08 ± 0.05	0.000 ± 0.007	-1.55 ± 0.10	2.87 ± 0.02	I
1.45	0.08 ± 0.07	0.000 ± 0.007	-1.41 ± 0.15	2.84 ± 0.03	I
1.50	0.02 ± 0.01	0.000 ± 0.006	-0.91 ± 0.07	2.72 ± 0.01	I
1.55	0.02 ± 0.01	0.000 ± 0.006	-0.60 ± 0.06	2.64 ± 0.01	I
1.60	0.02 ± 0.01	0.000 ± 0.006	-0.34 ± 0.06	2.57 ± 0.01	I

Table 2: Temperature dependence of the average fraction of particles belonging to columns $\langle x_c \rangle$, number of particles per column $\langle n_p \rangle$, and number of columns $\langle n_c \rangle$ from the MC–NPT simulations of the $N = 8192$ system. Estimated rms errors on the averages are ± 1 on the last digit.

T^*	$\langle n_c \rangle$	$\langle n_p \rangle$	$\langle x_c \rangle$
1.25	584.2	6.82	0.49
1.30	549.8	6.85	0.46
1.35	576.0	6.60	0.46
1.37	497.7	7.11	0.43
1.40	20.9	4.18	0.01
1.42	12.7	4.14	0.01
1.44	5.1	3.90	0.01
1.45	2.5	3.61	0.00
1.50	0.9	2.32	0.00
1.60	0.1	0.33	0.00

Table 3: Temperature dependence of the average fraction of columns organised into domains $\langle x_d \rangle$, number of domains $\langle n_d \rangle$, and number of columnar stacks per domain $\langle n_s \rangle$ from the MC-NPT simulations of the $N = 8192$ system. Estimated rms errors on the averages are ± 1 on the last digit.

T^*	$\langle n_d \rangle$	$\langle n_s \rangle$	$\langle x_d \rangle$
1.25	27.0	116.4	17.74
1.30	23.9	145.3	19.89
1.35	14.3	191.7	39.86
1.37	14.3	173.1	33.53
1.40	0.1	0.0	0.00
1.42	0.0	0.0	0.00
1.44	0.0	0.0	0.00
1.45	0.0	0.0	0.00
1.50	0.0	0.0	0.00
1.60	0.0	0.0	0.00

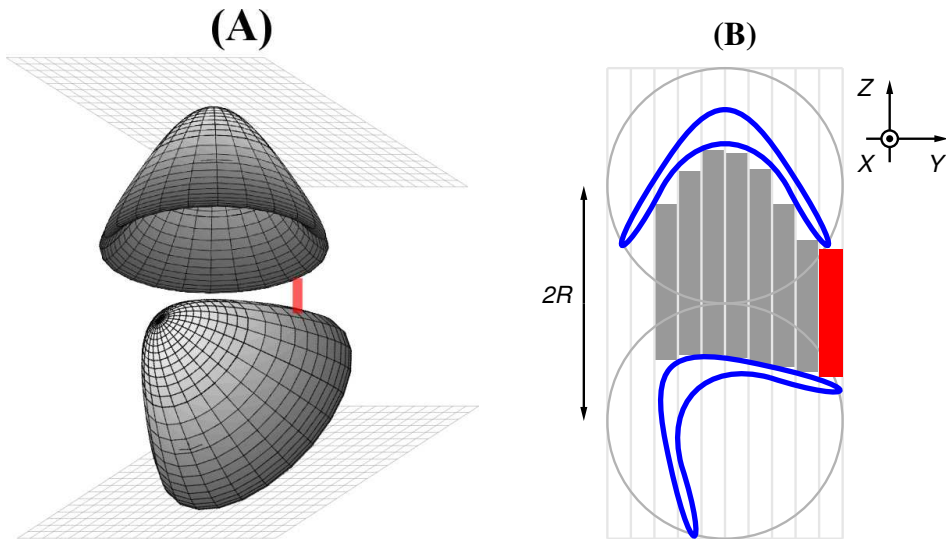


Figure 1: A schematic representation (scheme A) of the geometrical algorithm (see Ref. [24]) employed to generate a discrete approximation of the pair contact distance $\sigma(\mathbf{u}_1, \mathbf{u}_2, \mathbf{u}_r)$. As sketched in the cross section (scheme B) two particles with given orientations $\mathbf{u}_1, \mathbf{u}_2$ are enclosed by virtual spheres of radius R positioned at the centres of mass and tangent along the inter-particle position vector \mathbf{r}_{12} taken here parallel to the laboratory Z axis. The two molecular surfaces are mapped with a finite sampling grid to determine the minimum distance $\sigma_m = Z_2 - Z_1$ between pairs of points with the same X , and Y coordinates. The contact distance is computed as $\sigma(\mathbf{u}_1, \mathbf{u}_2, \mathbf{u}_r) = 2R - \sigma_m$.

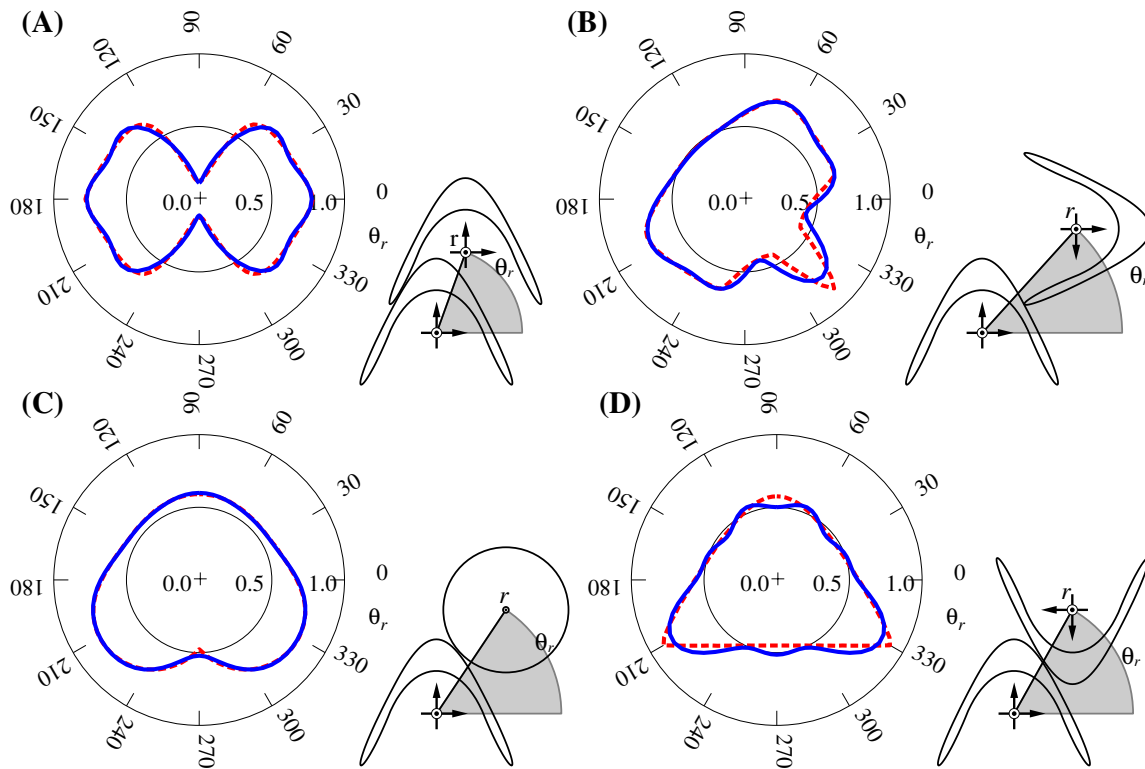


Figure 2: Contact distances profiles as computed from the algorithm described in Ref. [24] (blue solid lines) and from series expansion, eq. 1 (red dashed lines) for two bowl-shaped particles, for different configurations, as illustrated by the side sketches, with: (A) parallel, (B) tee, (C) cross, (D) antiparallel. The contact distance is represented as the radial distance from a particle kept fixed (both in position and orientation) at the origin, and a second one with fixed orientation, moving around the first one.

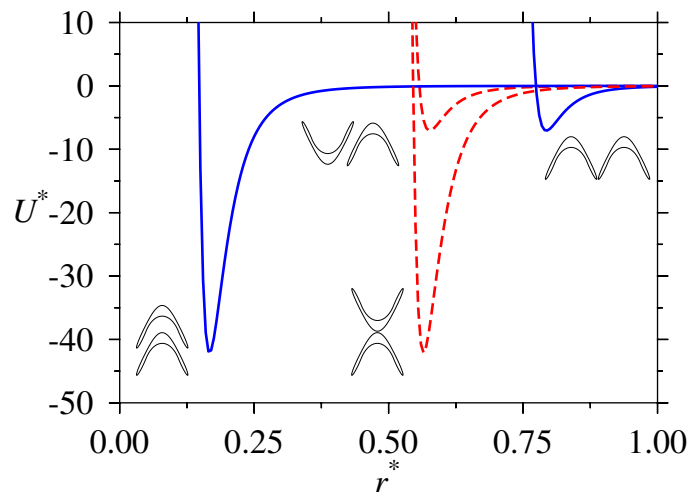


Figure 3: Distance dependence of the dimensionless pair interaction energy $U^* = U/\epsilon_0$ for a pair of bowl-shaped molecules with specific parallel (blue solid lines), and antiparallel (red dashed lines) relative orientations. The well depths for parallel or antiparallel configurations are the same, and the polarity in the potential stems only from the specific geometrical anisotropy (steric dipole).

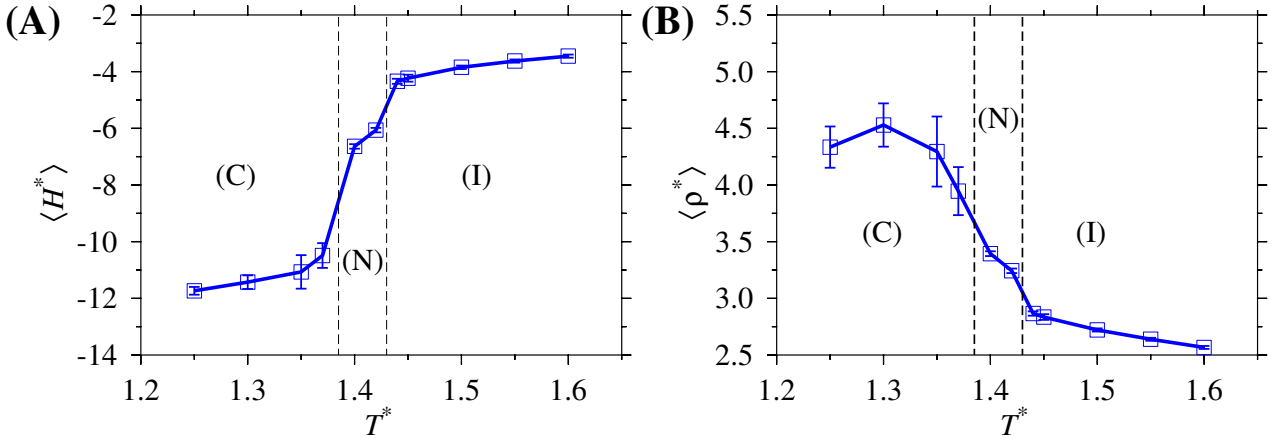


Figure 4: Dimensionless average enthalpy $\langle H^* \rangle = \langle H \rangle / \epsilon_0$ (plate A), and number density $\langle \rho^* \rangle = \sigma_0^3 N \langle 1/V \rangle$ (plate B) as a function of temperature from MC–NPT simulations at $P^* = 8$, for the system of $N = 8192$ molecules in the isotropic (I), nematic (N), and columnar (C) phases. The vertical dotted lines indicate the transition temperatures for the $N = 8192$ system, estimated as the midpoint between neighbouring phases.

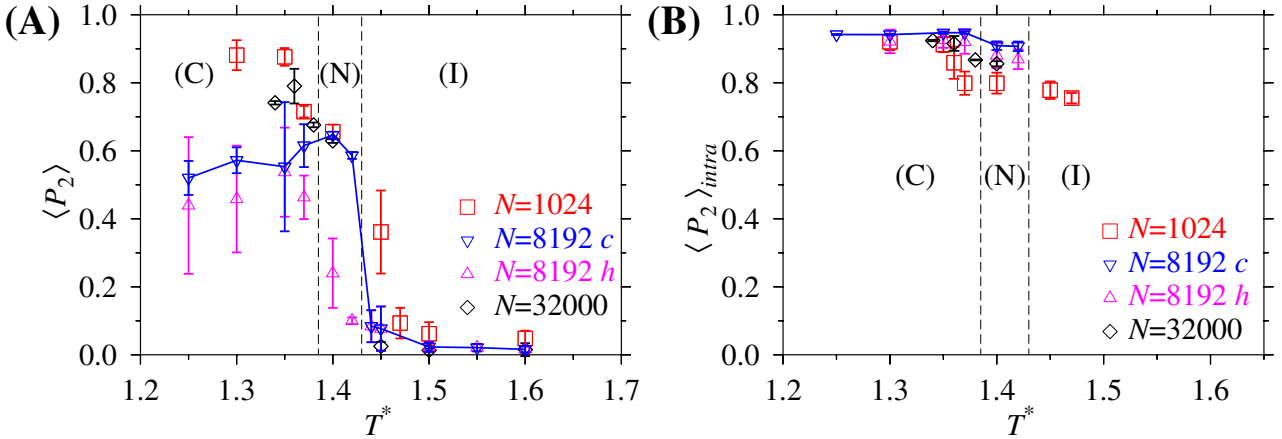


Figure 5: The average overall $\langle P_2 \rangle$ (plate A), and the intra–column $\langle P_2 \rangle_{\text{intra}}$ (plate B) orientational order parameters, as a function of dimensionless temperature from a cooling–down sequence of NPT Monte Carlo simulations of the $N = 1024$ (squares, red), $N = 8192$ (triangles down, blue) and $N = 32000$ (diamonds, black) molecules system, at dimensionless pressure $P^* = 8$, in the isotropic (I), nematic (N), and columnar (C) phases. The results obtained from the heating of an intermediate low–temperature $N = 8192$ sample (triangles up, magenta) are also plotted. The vertical dotted lines indicate the transition temperatures for the $N = 8192$ system, estimated as the midpoint between neighbouring phases.

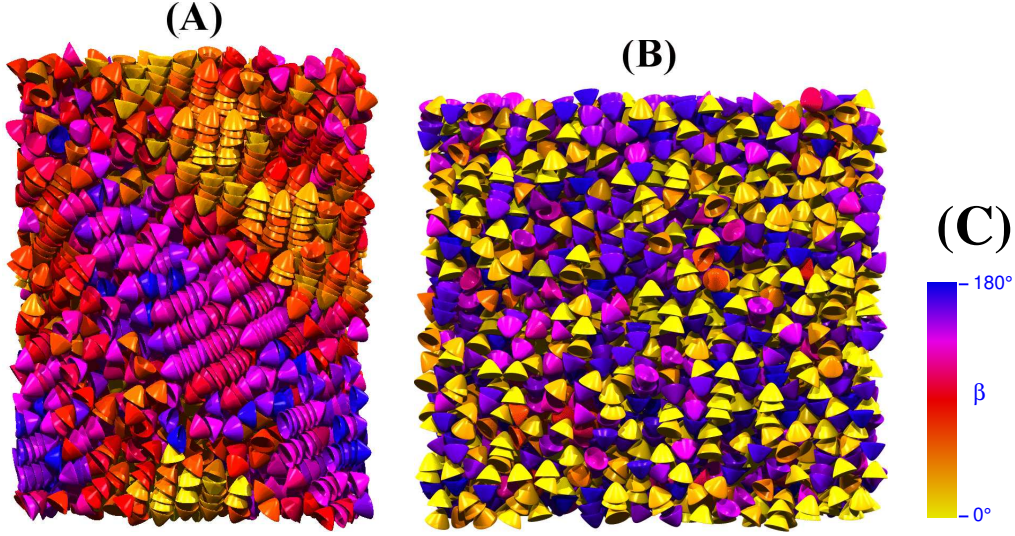


Figure 6: Snapshots obtained from MC–NPT simulations at $P^* = 8$ of the $N = 8192$ molecules sample. The polar domain organisations are clearly visible in the columnar sample simulated at $T^* = 1.3$ (plate A). In the snapshot of the nematic phase at $T^* = 1.42$ (plate B) no polar domains are present and only short stacks typically three–particles long can be found. The colour coding of the palette (plate C) refers the angle $\cos \beta = \mathbf{u}_i \cdot \mathbf{n}$ between particle orientations \mathbf{u}_i and mesophase director \mathbf{n} .

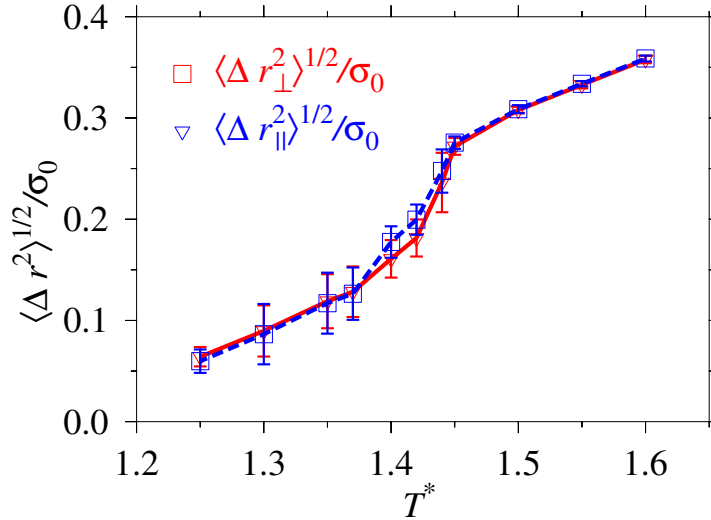


Figure 7: Dimensionless root mean square displacements $\langle \Delta r_{\parallel}^2 \rangle^{1/2} / \sigma_0$ (circles, blue), and $\langle \Delta r_{\perp}^2 \rangle^{1/2} / \sigma_0$ (squares, red) measured along the uniaxial director \mathbf{n} (parallel, \parallel), and with respect to an arbitrary orthogonal direction \mathbf{m} (perpendicular, \perp) from MC–NPT runs at $P^* = 8$, for the system of $N = 8192$ molecules.

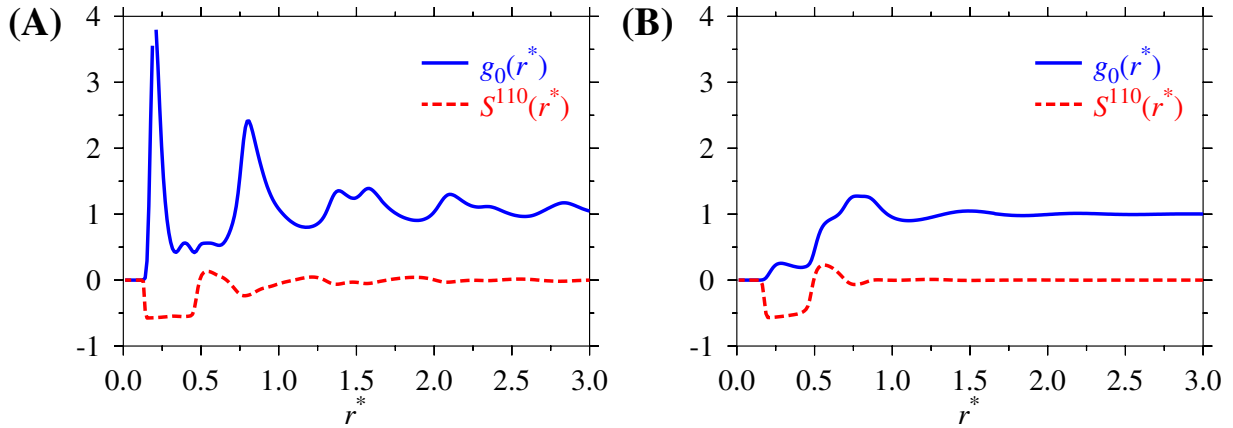


Figure 8: Average radial $g_0(r^*)$, and orientational $S^{110}(r^*)$ correlation functions at temperatures $T^* = 1.3$ (plate A) and $T^* = 1.42$ (plate B) corresponding to the columnar and nematic phases. The dimensionless intermolecular distance is $r^* = r/\sigma_0$.

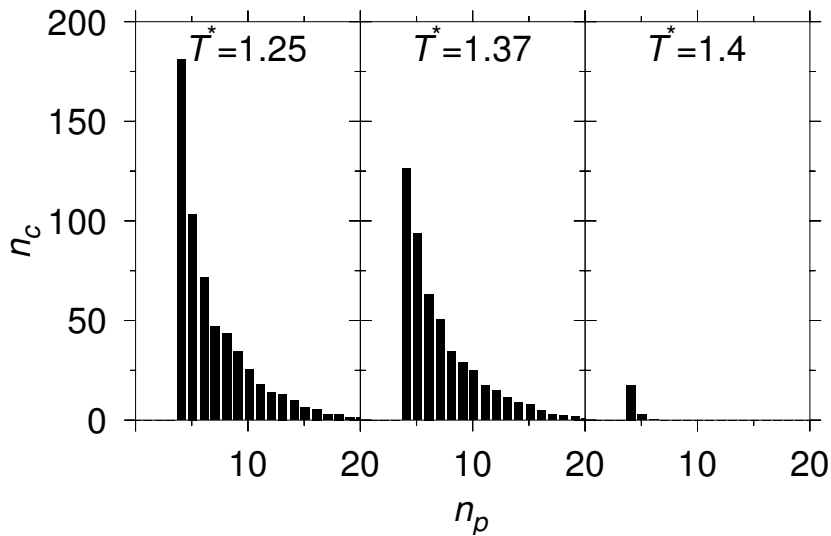


Figure 9: Distributions of the number of columns n_c formed by a number n_p of particles, at $T^* = 1.25$ (C), $T^* = 1.37$ (C), and $T^* = 1.4$ (N), from the MC-NPT simulations of the $N = 8192$ system.

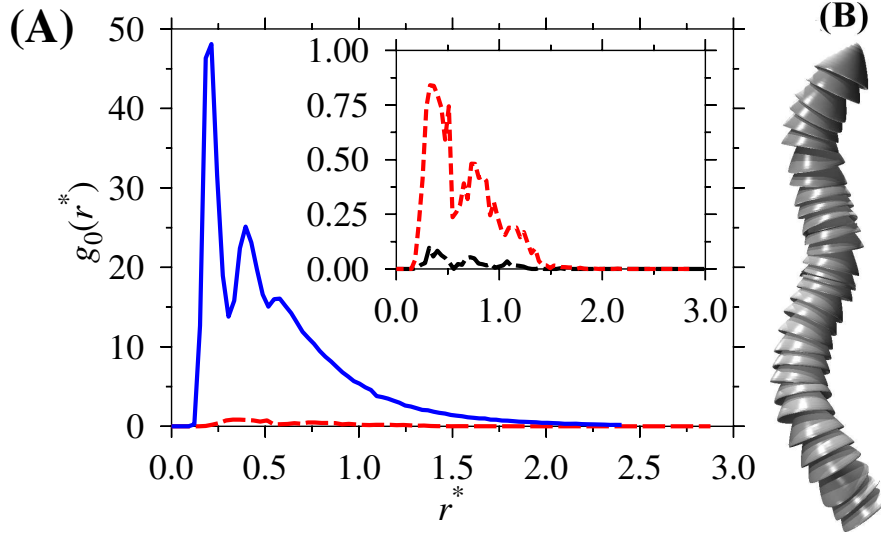


Figure 10: Average radial correlation function $g_0(r^*)$ (plate A) computed along columnar stacks (and normalised with respect to the number of columns), as a function of intermolecular distance r^* , at temperatures $T^* = 1.25$ (columnar phase, blue solid line), $T^* = 1.42$ (nematic phase, red short-dashed line), and $T^* = 1.5$ (isotropic phase, black long-dashed line). A snapshot of a winding stack of particles frequently found in the columnar phases is also shown (plate B).

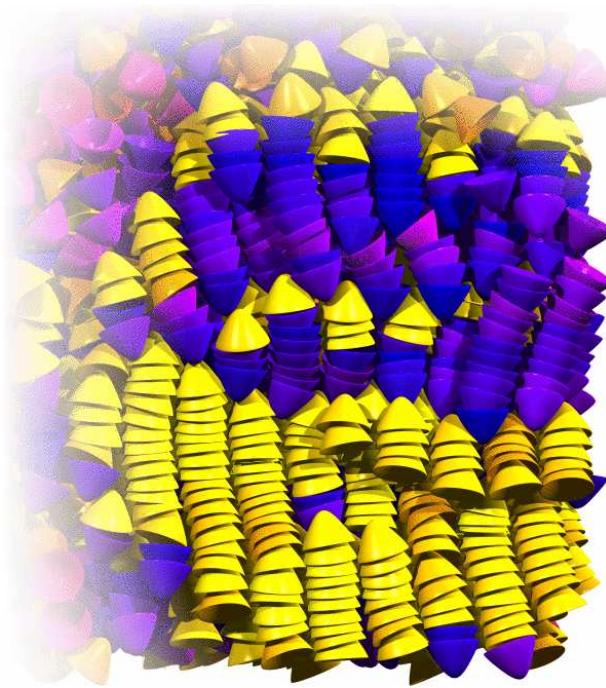


Figure 11: Detail of a $N = 8192$ columnar sample at $T^* = 1.37$ showing two polar domains formed by columns pointing upward (yellow), and downward (blue) with respect to the local mesophase director.

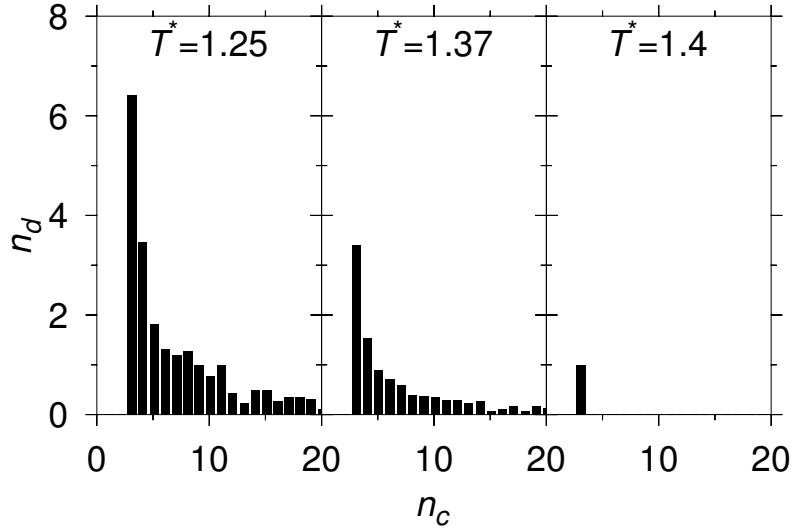


Figure 12: Distributions of the number of domains n_d with a given size, expressed as the number of columns n_c belonging to the domain itself, at $T^* = 1.25$ (C), $T^* = 1.37$ (C), and $T^* = 1.4$ (N), from the MC-NPT simulations of the $N = 8192$ system.

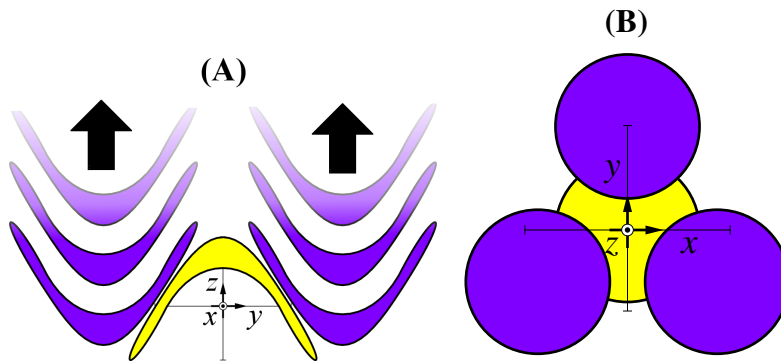


Figure 13: Geometrical sketches of lateral (scheme A), and top (scheme B) views of the typical boundary region separating polar columnar domains: an end-particle induces the terminal molecules of three neighbouring columns to be antiparallel (and vice-versa).

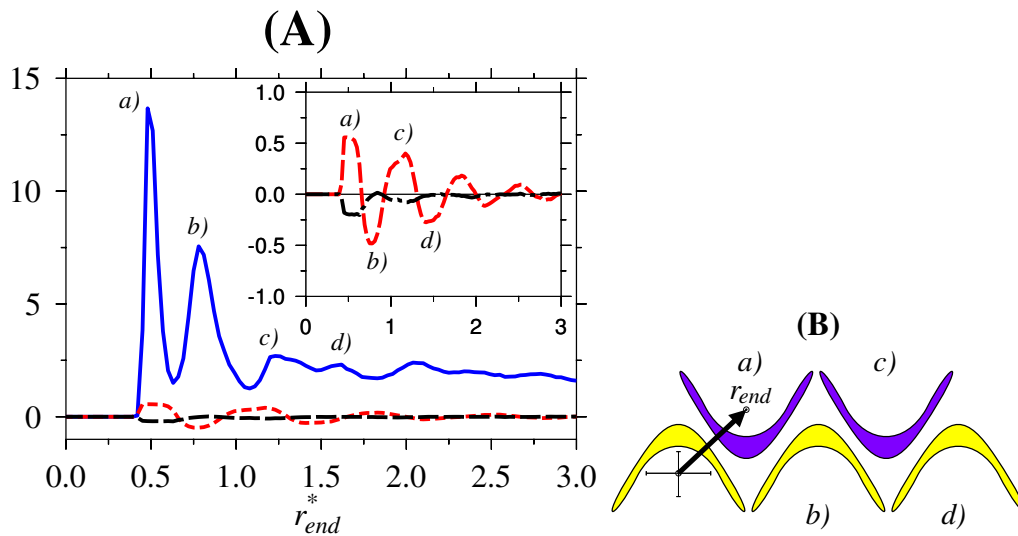


Figure 14: Average radial correlation function $g_0(r_{end}^*)$ (blue solid line), and orientational correlation function $S^{110}(r_{end}^*)$ between end-particles orientations (red short-dashed line), and $S^{101}(r_{end}^*)$ between particles and intermolecular vector orientations (black long-dashed line), for the columnar sample at $T^* = 1.3$ (plate A). The local maxima of the correlation functions are labelled according to the scheme B, where r_{end} is the distance between end-particles. To help in the visualisation, the short-range portions of the orientational correlations is enlarged in the inset of plate A.

Appendix

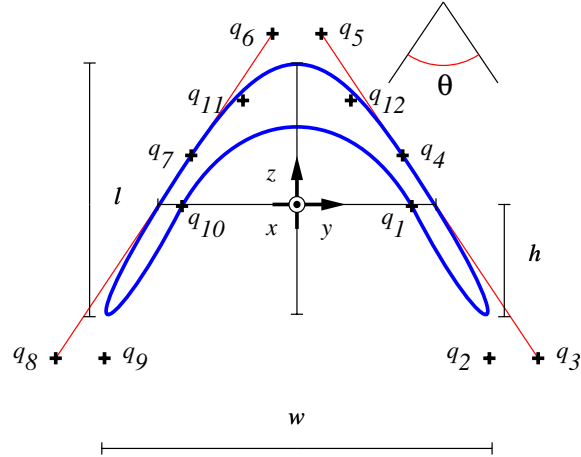


Figure A-1: A schematic cross-section of the uniaxial bowl-shaped particle (cut along the vertical $x = 0$ plane), with *length-to-width* ratio $l/w = 0.9$, *base-to-frame* ratio $h/l = 0.4$, and *top conic angle* $\theta = 34^\circ$ used to define the contact distance function whose approximation (as in Ref. [24]) enters into the generalised GB potential. The three-dimensional steric dipole is obtained by a 2π rotation about the molecular \mathbf{z} axis. The Bezier control points q_i are also shown (see Ref. [29]), and their positions with respect to the molecular frame axes are given in Table A-1.

q_i	y_i	z_i	q_i	y_i	z_i
q_1	0.24	0.00	q_2	0.39	-0.31
q_3	0.49	-0.31	q_4	0.22	0.10
q_5	0.05	0.35	q_6	-0.05	0.35
q_7	-0.22	0.10	q_8	-0.49	-0.31
q_9	-0.39	-0.31	q_{10}	-0.24	0.00
q_{11}	-0.11	0.22	q_{12}	0.11	0.22

Table A-1: The positions of the control points q_i defining the four Bezier parametric curves [29] used to model the vertical $x = 0$ cross section of Fig. A-1.

[000] = 0.05097	[011] = 0.01108	[101] = 0.01108	[112] = 0.00254
[121] = 0.00304	[211] = 0.00304	[132] = 0.01580	[312] = 0.01580
[143] = 0.00636	[233] = 0.00857	[323] = 0.00857	[413] = 0.00636
[154] = 0.00311	[235] = 0.00578	[244] = 0.00211	[325] = 0.00578
[334] = 0.01531	[343] = 0.00261	[424] = 0.00211	[433] = 0.00261
[514] = 0.00311	[165] = 0.00340	[336] = 0.03973	[345] = 0.00940
[354] = 0.00628	[435] = 0.00940	[462] = 0.00138	[534] = 0.00628
[552] = 0.00173	[615] = 0.00340	[642] = 0.00138	[176] = 0.00308
[266] = 0.00363	[347] = 0.01578	[356] = 0.00594	[365] = 0.00495
[437] = 0.01578	[446] = 0.00260	[536] = 0.00594	[563] = 0.00222
[626] = 0.00363	[635] = 0.00495	[653] = 0.00222	[716] = 0.00308
[277] = 0.00519	[367] = 0.00674	[448] = 0.01059	[637] = 0.00674
[727] = 0.00519	—	—	—

Table A–2: Explicit values of the 49 expansion coefficients $[L_1L_2L_3] \equiv \sigma_{L_1L_2L_3}$ used to approximate (with the procedure of Ref. [24]) the anisotropic contact distance between a pair of bowl-shaped particles obtained as a solid of rotation from the Bezier control points q_i of Table A–1.

List of all table captions

- Table 1** Average orientational order parameter $\langle P_2 \rangle$, dimensionless enthalpy $\langle H^* \rangle$, and number density $\langle \rho^* \rangle$ for the MC–NPT simulations of the $N = 8192$ system giving isotropic (I), nematic (N), and columnar (C) phases as indicated. Estimated rms errors on the averages (sampling a configuration every 20 MC cycles) are also given.
- Table 2** Temperature dependence of the average fraction of particles belonging to columns $\langle x_c \rangle$, number of particles per column $\langle n_p \rangle$, and number of columns $\langle n_c \rangle$ from the MC–NPT simulations of the $N = 8192$ system. Estimated rms errors on the averages are ± 1 on the last digit.
- Table 3** Temperature dependence of the average fraction of columns organised into domains $\langle x_d \rangle$, number of domains $\langle n_d \rangle$, and number of columnar stacks per domain $\langle n_s \rangle$ from the MC–NPT simulations of the $N = 8192$ system. Estimated rms errors on the averages are ± 1 on the last digit.
- Table A–1** The positions of the control points q_i defining the four Bezier parametric curves [29] used to model the vertical $x = 0$ cross section of Fig. A–1.
- Table A–2** Explicit values of the 49 expansion coefficients $[L_1 L_2 L_3] \equiv \sigma_{L_1 L_2 L_3}$ used to approximate (with the procedure of Ref. [24]) the anisotropic contact distance between a pair of bowl-shaped particles obtained as a solid of rotation from the Bezier control points q_i of Table A–1.

List of all figure captions

- Figure 1** A schematic representation (scheme A) of the geometrical algorithm (see Ref. [24]) employed to generate a discrete approximation of the pair contact distance $\sigma(\mathbf{u}_1, \mathbf{u}_2, \mathbf{u}_r)$. As sketched in the cross section (scheme B) two particles with given orientations $\mathbf{u}_1, \mathbf{u}_2$ are enclosed by virtual spheres of radius R positioned at the centres of mass and tangent along the inter-particle position vector \mathbf{r}_{12} taken here parallel to the laboratory Z axis. The two molecular surfaces are mapped with a finite sampling grid to determine the minimum distance $\sigma_m = Z_2 - Z_1$ between pairs of points with the same X , and Y coordinates. The contact distance is computed as $\sigma(\mathbf{u}_1, \mathbf{u}_2, \mathbf{u}_r) = 2R - \sigma_m$.
- Figure 2** Contact distances profiles as computed from the algorithm described in Ref. [24] (blue solid lines) and from series expansion, eq. 1 (red dashed lines) for two bowl-shaped particles, for different configurations, as illustrated by the side sketches, with: (A) parallel, (B) tee, (C) cross, (D) antiparallel. The contact distance is represented as the radial distance from a particle kept fixed (both in position and orientation) at the origin, and a second one with fixed orientation, moving around the first one.
- Figure 3** Distance dependence of the dimensionless pair interaction energy $U^* = U/\epsilon_0$ for a pair of bowl-shaped molecules with specific parallel (blue solid lines), and antiparallel (red dashed lines) relative orientations. The well depths for parallel or antiparallel configurations are the same, and the polarity in the potential stems only from the specific geometrical anisotropy (steric dipole).
- Figure 4** Dimensionless average enthalpy $\langle H^* \rangle = \langle H \rangle / \epsilon_0$ (plate A), and number density $\langle \rho^* \rangle = \sigma_0^3 N \langle 1/V \rangle$ (plate B) as a function of temperature from as a function of temperature from MC-NPT simulations at $P^* = 8$, for the system of $N = 8192$ molecules in the isotropic (I), nematic (N), and columnar (C) phases. The vertical dotted lines indicate the transition temperatures for the $N = 8192$ system, estimated as the midpoint between neighbouring phases.
- Figure 5** The average overall $\langle P_2 \rangle$ (plate A), and the intra-column $\langle P_2 \rangle_{\text{intra}}$ (plate B) orientational order parameters, as a function of dimensionless temperature from a cooling-down sequence of NPT Monte Carlo simulations of the $N = 1024$ (squares, red), $N = 8192$ (triangles down, blue) and $N = 32000$ (diamonds, black) molecules system, at dimensionless pressure $P^* = 8$, in the isotropic (I), nematic (N), and columnar (C) phases. The results obtained from the heating of an intermediate low-temperature $N = 8192$ sample (triangles up, magenta) are also plotted. The vertical dotted lines indicate the transition temperatures for the $N = 8192$ system, estimated as the midpoint between neighbouring phases.
- Figure 6** Snapshots obtained from MC-NPT simulations at $P^* = 8$ of the $N = 8192$ molecules sample. The polar domain organisations are clearly visible in the columnar sample simulated at $T^* = 1.3$ (plate A). In the snapshot of the nematic phase at $T^* = 1.42$ (plate B) no polar domains are present and only short stacks typically three-particles long can be found. The colour coding of the palette (plate C) refers the angle $\cos \beta = \mathbf{u}_i \cdot \mathbf{n}$ between particle orientations \mathbf{u}_i and mesophase director \mathbf{n} .
- Figure 7** Dimensionless root mean square displacements $\langle \Delta r_{\parallel}^2 \rangle^{1/2} / \sigma_0$ (circles, blue), and $\langle \Delta r_{\perp}^2 \rangle^{1/2} / \sigma_0$ (squares, red) measured along the uniaxial director \mathbf{n} (parallel, \parallel), and

with respect to an arbitrary orthogonal direction \mathbf{m} (perpendicular, \perp) from MC–NPT runs at $P^* = 8$, for the system of $N = 8192$ molecules.

Figure 8 Average radial $g_0(r^*)$, and orientational $S^{110}(r^*)$ correlation functions at temperatures $T^* = 1.3$ (plate A) and $T^* = 1.42$ (plate B) corresponding to the columnar and nematic phases. The dimensionless intermolecular distance is $r^* = r/\sigma_0$.

Figure 9 Distributions of the number of columns n_c formed by a number n_p of particles, at $T^* = 1.25$ (C), $T^* = 1.37$ (C), and $T^* = 1.4$ (N), from the MC–NPT simulations of the $N = 8192$ system.

Figure 10 Average radial correlation function $g_0(r^*)$ (plate A) computed along columnar stacks (and normalised with respect to the number of columns), as a function of intermolecular distance r^* , at temperatures $T^* = 1.25$ (columnar phase, blue solid line), $T^* = 1.42$ (nematic phase, red short-dashed line), and $T^* = 1.5$ (isotropic phase, black long-dashed line). A snapshot of a winding stack of particles frequently found in the columnar phases is also shown (plate B).

Figure 11 Detail of a $N = 8192$ columnar sample at $T^* = 1.37$ showing two polar domains formed by columns pointing upward (yellow), and downward (blue) with respect to the local mesophase director.

Figure 12 Distributions of the number of domains n_d with a given size, expressed as the number of columns n_c belonging to the domain itself, at $T^* = 1.25$ (C), $T^* = 1.37$ (C), and $T^* = 1.4$ (N), from the MC–NPT simulations of the $N = 8192$ system.

Figure 13 Geometrical sketches of lateral (scheme A), and top (scheme b) views of the typical boundary region separating polar columnar domains: an end-particle induces the terminal molecules of three neighbouring columns to be antiparallel (and vice-versa).

Figure 14 Average radial correlation function $g_0(r_{end}^*)$ (blue solid line), and orientational correlation function $S^{110}(r_{end}^*)$ between end-particles orientations (red short-dashed line), and $S^{101}(r_{end}^*)$ between particles and intermolecular vector orientations (black long-dashed line), for the columnar sample at $T^* = 1.3$ (plate A). The local maxima of the correlation functions are labelled according to the scheme B, where r_{end} is the distance between end-particles. To help in the visualisation, the short-range portions of the orientational correlations is enlarged in the inset of plate A.

Figure A–1 A schematic cross-section of the uniaxial bowl-shaped particle (cut along the vertical $x = 0$ plane), with *length-to-width* ratio $l/w = 0.9$, *base-to-frame* ratio $h/l = 0.4$, and *top* conic angle $\theta = 34^\circ$ used to define the contact distance function whose approximation (as in Ref. [24]) enters into the generalised GB potential. The three-dimensional steric dipole is obtained by a 2π rotation about the molecular \mathbf{z} axis. The Bezier control points q_i are also shown (see Ref. [29]), and their positions with respect to the molecular frame axes are given in Table A–1.